High performance porphyrin-based dye-sensitized solar cells with both iodine and cobalt redox shuttles

FULL PAPER

High performance porphyrin-based dye-sensitized solar cells with both iodine and cobalt redox shuttles

Huaide Xiang,[†][a] Wei Fan, [†][b] Jia Hui Li,[c] Tianyue Li,[d] Neil Robertson,[d] Xiongrong Song,[a] Wenjun Wu,*[a] Zhaohui Wang,[b] Weihong Zhu,[a] and He Tian*[a]

Abstract: Recently, enormous research passion has been devoted to enhance the power conversion efficiency (PCE) of porphyrin sensitizers for DSSCs, but the major stumbling block is its absorption defects in visible spectrum region. To address the challenge, herein we reported a duplexing high performance photovoltaic result for DSSCs based on a novel D-*π*-A sensitizer **FW-1** 7H-Dibenzo[*c,g*] carbazole-substituted and fused Zn-porphyrin, co-sensitized with benzotriazole featured dye (**WS-5**) in iodine and cobalt redox system and got high PCE of 10.21% and 10.42%, respectively. An unprecedented breakthrough was got for supplying the gap of one sensitizer suitable for more electrolyte systems due to the appropriate molecular orbitals and co-sensitizer.

Introduction

Since Grätzel and O'Regan first reported ruthenium (Ru) based sensitizers in 1991,[1] dye-sensitized solar cells (DSSCs) have been the centre of widespread interest owing to their outstanding performance.[2,3] The past decade has witnessed rapid development in the syntheses and applications of porphyrin dyes, as the photosensitizer is crucial to determine the power conversion efficiency (PCE) of DSSCs. In this respect, zinc-based porphyrin dyes, with high molar extinction coefficients and strong absorption in a broad wavelength range may be suitable for wild-ranging applications.[4] To date, Grätzel *et al.* have reported the highest PCE of 13.0% for porphyrin sensitizer SM315 with cobalt electrolyte.[5] However, porphyrin dyes show typical absorbing defects in the regions of 350–410 nm and 500–600 nm, which is one of the major stumbling blocks restricting the enhancement of PCE.

To address the challenge, the co-sensitization method, utilizing co-sensitizers to simultaneously fill up the porphyrin absorption valleys, becomes an attractive choice. Recently, fascinating investigations have converged on a series of novel D–A–*π*–A indoline dyes with auxiliary acceptors as superior sensitizers in DSSCs (**WS** series).[6] Among these dyes, **WS-5**,[7] with high light-harvesting capability in the regions of 350–420 nm and 450–650 nm, has led to promising PCEs through application in co-sensitization systems.[8] Through co-sensitization using small dye **WS-5**, a new record efficiency of 11.5% based on iodine electrolyte was achieved.[9] Typically however, any given sensitizer is usually most compatible with a single electrolyte system for the best efficiency, and there remains no examples achieving high PCE for the same kind of sensitizers based on both iodine and cobalt redox electrolytes.

With these concerns in mind, herein we have developed a novel D-*π*-A 7H-Dibenzo[*c,g*]carbazole and fused Zn-porphyrin (**FW-1**) with unique molecular structure (Scheme 1). 7*H*-*D*ibenzo[*c,g*]carbazole serves as electron donor, Zn-porphyrin as π-spacer and benzoic acid as acceptor, thus a "push-pull" structure is produced. Furthermore, long alkyl chains as well as o-alkoxy-substituted phenyl groups were chosen to surmount the solubility problem and reduce dye aggregation, which contributes to the extraordinary photovoltaic performance. Due to its complementary absorption spectra, **WS-5** was selected as co-sensitizer for **FW-1**. Electrochemical impedance spectroscopy (EIS) and open-circuit voltage decay (OCVD) investigations were performed to understand the influence of co-sensitization on V_{OC}. As a result, compared to the single sensitizer **FW-1**, **FW-1 + WS-5** shows a breakthrough of PCE from 6.53% and 7.05% to 10.22% and 10.42% based on I^-/I_3^- and Co(II/III) electrolyte, respectively, and additionally 10.80% under 0.79 sun irradiation with the latter electrolyte (Table S3 †). To the best of our knowledge, this is the first time that PCEs are reported exceeding 10% for a porphyrin dye based on different redox shuttles, hence **FW-1 + WS-5** offers a new avenue for basic understanding and also the practical development of DSSCs.

Results and Discussion

Figure 1a shows the absorption spectra of **FW-1** and **WS-5** in THF solution. **FW-1** exhibits typical porphyrin absorption characteristics with a strong Soret band in the range of 400–500 nm and moderate Q-bands in the range of 600–700 nm, but very weak absorption between 350–400 nm and 500–600 nm.

[a] *H. Xiang, X. Song, Dr. W. Wu, Prof. W. Zhu, Prof. H. Tian*
Key Laboratory for Advanced Materials and Institute of Fine Chemicals
East China University of Science and Technology
130 Meilong Road, Shanghai, 200237, China.
E-mail: wjwu@ecust.edu.cn, tianhe@ecust.edu.cn.
[b] *W. Fan, Prof. Z. Wang*
Key Laboratory of Organic Solids, Beijing National Laboratory for Molecular Sciences
Institute of Chemistry, Chinese Academy of Sciences
Beijing 100190, China.
[c] *J. H. Li*
Sino-German College of Technology
East China University of Science and Technology
130 Meilong Road, Shanghai, 200237, China.
[d] *T. Li, Prof. N. Robertson*
EaStCHEM School of Chemistry
University of Edinburgh
Kings Buildings, Edinburgh EH9 3FJ, UK.

† These authors contributed equally to this work.
Supporting information for this article is given via a link at the end of the document.

Distinctively, **WS-5** exhibits strong absorption in the range of 350–600 nm, which compensates the absorption valleys of **FW-1**. Illustrating this, absorption spectra of **FW-1, WS-5** and **FW-1 + WS-5** onto TiO_2 films were performed (Figure 1b), with a similar trend compared to Figure 1a. The absorption bands of both dyes are broadened, although the absorption peaks of **FW-1** and **WS-5** are blue-shifted (10 and 15 nm, respectively). Upon co-sensitization with **FW-1** and **WS-5** on the TiO_2 film, the absorption spectrum of **FW-1** is complemented by **WS-5**, showing a strong absorption spectrum from 350 nm to 600 nm. Therefore, we are pleased to find that **WS-5** serves as a perfect co-sensitizer for **FW-1**. What's more, the absorbance as a function of dipping time was measured for **FW-1** and **WS-5** to optimize the co-sensitization procedure. As depicted in Figure 1c and 1d, **FW-1** needs 12 h to reach its saturated mode, while for **WS-5**, the saturated adsorption duration is only around 6 h, showing a much faster adsorption rate with respect to **FW-1**. This shows that **WS-5** is much more readily adsorbed onto the TiO_2 surface.

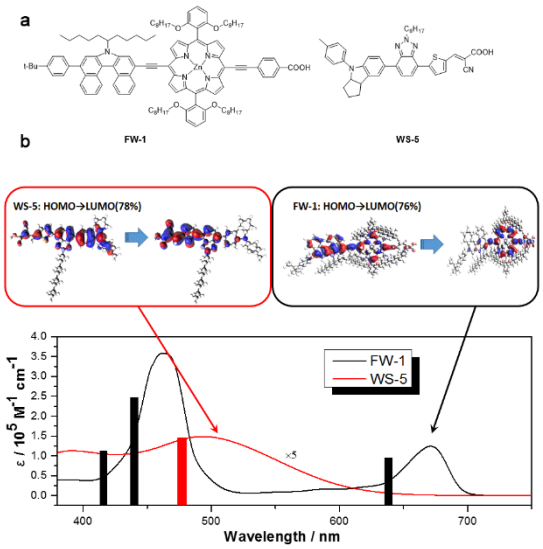

Scheme 1. a) Molecular structures and b) computational absorption spectrum of dyes **FW-1** and **WS-5**.

As is well-known, suitable HOMO and LUMO energy levels are also critical parameters for the electron injection and dye regeneration processes. Cyclic voltammograms were performed in CH_2Cl_2 solution to evaluate the redox potentials (Figure S1†) with ferrocene (0.64 V *vs.* normal hydrogen electrode, NHE) as external reference (Table S1†). The first oxidation potentials (E_{ox}) of **FW-1** and **WS-5** are 1.00 and 1.09 V, respectively, higher than those of I^-/I_3^- (0.4 V *vs.* NHE) and $Co(bpy)_3^{2+/3+}$ (0.57 V *vs.* NHE),[10] which ensures ample driving force for oxidized dye regeneration. The excited-state reduction potentials (E_{red}*) of **FW-1** and **WS-5** are determined according to the equation of $E_{red}^* = E_{OX} - E_{0-0}$. Consequently, the E_{red}* of **FW-1** and **WS-5** (−1.09 and −1.45 V) are more negative than the conduction band (E_{CB}) of TiO_2 electrode (−0.5 V *vs.* NHE), indicating that the electron injection process from the excited dye into the conduction band of TiO_2 is energetically permitted. This verifies that the generation and separation of photo-excited electrons and dye regeneration processes are thermodynamically favourable for **FW-1** and **WS-5**.

DFT calculations were carried out to investigate the electronic structures of **WS-5** and **FW-1**, and selected Kohn-Sham (KS) molecular orbital distributions were visualized. For **FW-1**, the KS highest occupied molecular orbital (HOMO) is mainly located on the electron donating group of 7H-Dibenzo[*c,g*]carbazole, with some distribution on the Zn-porphyrin group. The location for the KS lowest unoccupied molecule orbital (LUMO) is on both of Zn-porphyrin π-spacer and benzoic acid group, serving as electron acceptor. For the co-sensitizer **WS-5**, the HOMO and LUMO are located on the indoline group and cyanoacetic acid group, respectively. The calculated molecular orbital energies for both dyes in THF solvent are shown in table S4 and S6.

According to Time-dependent DFT (TD-DFT) calculation results, comparison of experimental and computational absorption spectrum can be studied and investigated (Scheme 1b). The calculated absorption spectrum shows good agreement with the experimental one, which helps to clarify the pathways of excitation and electron injection processes. Results of TD-DFT calculated absorption energies and compositions of selected transitions are shown in table S5. The first electronic transition of **FW-1** characterized by HOMO → LUMO contribution (76%) was calculated to be at 638 nm, and the absorption calculated at 440 nm is characterized by HOMO-1 → LUMO+1 (49%). The absorption valley of **FW-1** is well compensated by the co-sensitizer **WS-5** and this is illustrated computationally, showing the first electronic transition at 477 nm (78% contributed by HOMO → LUMO transition of **WS-5**).

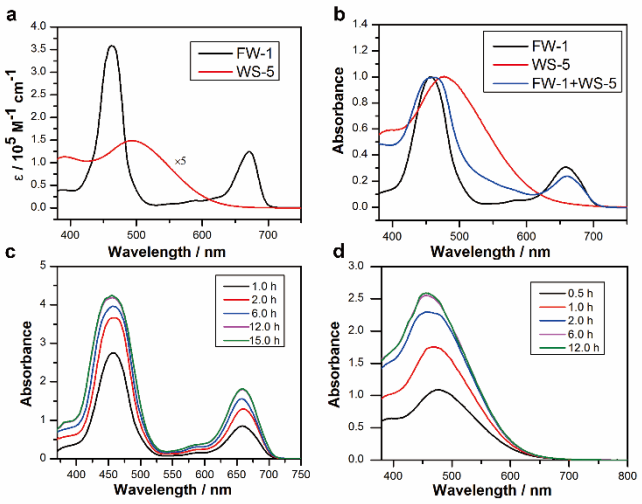

Figure 1. (a) Absorption spectra of **FW-1** and **WS-5** in THF solution, (b) **FW-1**, **WS-5** and co-sensitizer (**FW-1**+**WS-5**) adsorbed onto 3 μm transparent TiO_2 films and absorbance as a function of dipping time for (c) **FW-1**, (d) **WS-5** on a 12 μm transparent TiO_2 film.

The DSSC performances of **FW-1** and **FW-1**+**WS-5** with different electrolytes were tested under AM 1.5 G irradiation (100 mW cm^{-2}), and the photovoltaic parameters are presented in

Table 1, with more details listed in Tables S2 and 3†. Figure 2 illustrates *J–V* characteristics of **FW-1**+**WS-5** co-sensitized DSSCs with different **WS-5** dipping time based on the I^-/I_3^- and $[Co(bpy)_3]^{2+/3+}$ electrolytes, respectively. It is observed that V_{OC} of **FW-1** devices with cobalt electrolyte is higher than that with iodine electrolyte by 176 mV, while showing a lower J_{SC} of 11.5 mA cm^{-2} compared to 14.14 mA cm^{-2}. Moreover, we investigated and optimized the co-sensitization procedure for different redox electrolytes. First, we recorded the effects of **FW-1**-sensitized TiO_2 dipped in **WS-5** solution for different time based on iodine redox shuttle (Table S2†). As a result, after co-sensitizing with **WS-5** for only 0.5 h, J_{SC} increases significantly from 14.10 to 19.35 mA cm^{-2}. Along with the increase of dipping time from 0.5 to 1.5 h, J_{SC} reaches 19.91 mA cm^{-2}. The improvement in J_{SC} is mainly attributed to the complementary light response of **FW-1**. However, J_{SC} decreases when dipping time extends to 1.5 h. After co-sensitizing for 2.5 h, J_{SC} decreases to 17.7 mA cm^{-2}, which can be explained in that a significant quantity of **FW-1** is replaced by **WS-5**, finally resulting in the huge decrease of IPCE in the long wavelength region (Figure 2c). In addition, V_{OC} plays a pivotal role in the development of DSSCs and along with the increase of dipping time from 0 to 2.5 h, V_{OC} increases from 699 to 783 mV. Consequently, an excellent PCE of 10.21% (V_{OC} of 761mV, J_{SC} of 18.90 mA cm^{-2} and FF of 0.71) is achieved under irradiation of AM 1.5 simulated solar light (100 mW cm^{-2}). In the case of cobalt-based electrolyte, after 2 h of adsorption in **FW-1** and the increase of dipping time in **WS-5** (Table S3†), we find the same trend in J_{SC}, with a great increase from 11.50 to 18.25 mA cm^{-2}. However, when the dipping time extends over 1.5 h, J_{SC} decreases to 17.17 mA cm^{-2}. In the meantime, it is intriguing to note that the trend of V_{OC} with cobalt-based electrolyte is opposite to that of iodine-based electrolyte, showing a slight decrease of V_{OC} from 876 to 837 mV. As a result, a satisfactory PCE of 10.42 % (V_{OC} of 840mV, J_{SC} of 18.25 mA cm^{-2} and FF of 0.68) is achieved for 1.5 h **WS-5** adsorption time.

Table 1. Photovoltaic performance of **FW-1** and **FW-1 + WS-5** based DSSCs under irradiation of AM 1.5 simulated solar light (100 mW cm^{-2})

Dye	Electrolyte	J_{SC} (mA cm^{-2})	V_{OC} (mV)	FF	η (%)
FW-1	$[Co(bpy)_3]^{2+/3+}$	11.50±0.11	876±3	0.70±0.01	7.05±0.1
WS-5	$[Co(bpy)_3]^{2+/3+}$	13.58±0.17	821±5	0.68±0.03	7.58±0.2
FW-1+WS-5	$[Co(bpy)_3]^{2+/3+}$	18.25±0.29	840±4	0.68±0.01	10.42±0.1
FW-1	I^-/I_3^-	14.14±0.07	700±4	0.66±0.01	6.53±0.2
WS-5	I^-/I_3^-	16.17±0.15	792±6	0.68±0.01	8.71±0.1
FW-1+WS-5	I^-/I_3^-	18.90±0.24	761±2	0.71±0.01	10.21±0.1

In an effort to provide a further insight into the co-sensitized devices, we studied the incident photon-to-current conversion efficiency (IPCE) spectra to understand the contribution of co-sensitization on J_{SC} with two different redox electrolytes. As shown in Figure 2c and 2d, two IPCE valleys of **FW-1** are located in the ranges of 350–410 nm and 500–600 nm, respectively. Compared to the cobalt electrolyte, a higher IPCE of **FW-1**-based iodine redox electrolyte is found. In addition, the IPCE values of **WS-5** is above 70% within a wide range of wavelength, proving evidently that **WS-5** serves as a perfect co-sensitizer for **FW-1** by filling up both of the absorption valleys. As a result, the IPCE valleys of **FW-1** around 350 nm and 550 nm are indeed filled up, with IPCE values lying above 80% roughly within a wide wavelength range of 380–580 nm using iodine and cobalt redox electrolytes, respectively. We note that J_{SC} estimated from IPCE spectra are slightly smaller than those obtained from the *J–V* curves. Integration of IPCE curve for **FW-1** + **WS-5** with iodine redox electrolyte affords a calculated J_{SC} of 17.76 mA cm^{-2}, which is slightly lower than the experimental value of 18.90 mA cm^{-2}. Similar observations have also been reported for a number of porphyrin dyes.[11] These observations may be interpreted in terms of more efficient charge transport and collection[12] and stronger thermal effect associated with the full sunlight irradiation [13] and the weak current produced by diffuse light during the *J-V* measurement.

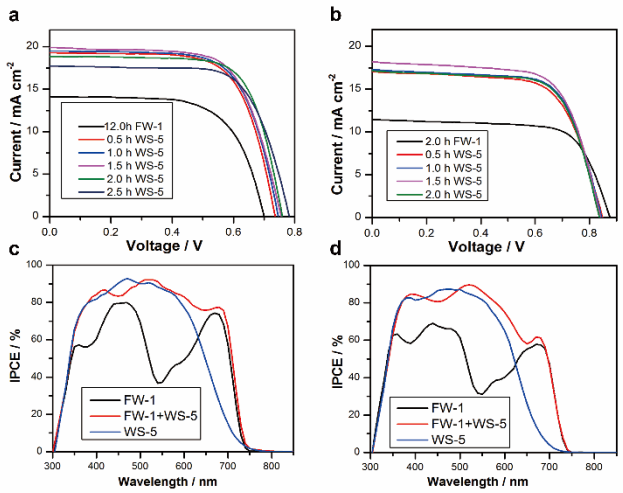

Figure 2. *J–V* characteristics of **FW-1**+**WS-5** sensitized DSSCs for different dipping time of **WS-5** based on iodine (a) or cobalt (b) redox electrolyte; IPCE spectra of DSSCs sensitized with **FW-1**, **WS-5** and **FW-1**+**WS-5** based on iodine (c) or (d) cobalt redox electrolyte.

Particularly, for iodine-based devices, along with the increase of dipping time of **WS-5** from 0 to 2.5 h, V_{OC} increases from 700 to 783 mV. It is well acknowledged that, with the use of fixed redox species, V_{OC} is only determined by Fermi level (E_{Fn}) of TiO_2, which is affected by conduction band (E_{CB}) and charge recombination rate.[14] To gain insight into the effect of co-sensitization on V_{OC}, **FW-1** and **FW-1** + **WS-5** sensitized DSSCs were characterized by electrochemical impedance spectroscopy (EIS). As derived from Figure 3a, the logarithm of chemical capacitance, C_μ, increases linearly with increasing bias potential and exhibits the same slope and values with the variation of electrolyte, indicating that E_{CB} of both devices are at the same level. However, compared to **FW-1**,

FW-1 + WS-5 presents a longer lifetime (Figure 3b), which we attribute to the introduction of co-sensitizer **WS-5** suppressing the charge recombination on the surface of TiO_2. Figure 3c shows the representative V_{OC} decay curves of **FW-1** and **FW-1** + **WS-5** devices, which remarkably reflect the charge recombination rate in devices. Apparently, the V_{OC} decay rate of **FW-1** cell is much higher than that of **FW-1**+**WS-5** cell, showing lower recombination rate for co-sensitized DSSCs, which is in good agreement with the EIS result. The prolonged electron lifetime through co-sensitization is beneficial for suppressing the charge recombination rate and results in the enhancement in V_{OC}.

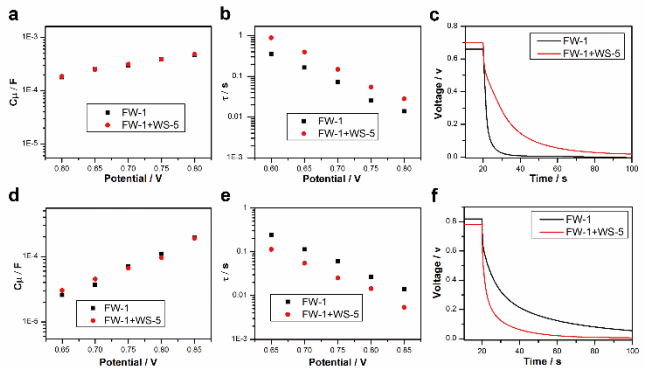

Figure 3. Curves under a series of potential bias of DSSCs based on reference dyes **FW-1** and **FW-1**+**WS-5** with iodine redox electrolyte: (a) cell capacitance (C_μ), (b) calculated electron lifetime (τ) and (c) V_{OC} decay curves of the **FW-1** and **FW-1**+**WS-5**; and with cobalt redox electrolyte: (d) cell capacitance (C_μ), (e) calculated electron lifetime (τ) and (f) V_{OC} decay curves of the **FW-1** and **FW-1**+**WS-5**.

In case of the cobalt redox electrolytes, conversely, V_{OC} of **FW-1**+**WS-5** device decreases with the increase of the dipping time of co-sensitizer, while C_μ of both devices are the same (Figure 3d), indicating that E_{CB} of **FW-1** and **FW-1**+**WS-5** are also at the same level. Meanwhile, the lifetime trend is **FW-1** > **FW-1** + **WS-5**, following the order of V_{OC}. As shown in Figure 3e, the electron lifetime of **FW-1** + **WS-5** decreases compared to that of individual sensitized device. Moreover, its OCVD dynamics are also presented in Figure 3f. It shows that higher recombination rate for the **FW-1** + **WS-5**-based DSSCs with cobalt electrolyte. As a one electron transfer system, the electron recombination with cobalt redox electrolyte is more facile than that with the two-electron transfer iodine-based electrolyte, especially in thinner films, and the lack of bigger donor will benefit the approach of cobalt complexes closer to the TiO_2 surface. Compared to iodine redox shuttle, **WS-5** with the smaller donor indoline is not conducive to suppress the charge recombination of co-sensitized system in the presence of cobalt-based one. In contrast, it just aggravated the charge recombination of co-sensitized system relative to individual dye-sensitized system, resulting the decrease of V_{OC} [17, 18].

As an interesting discovery, the specific structure of **FW-1** determines that E_{CB} remains the same in two different electrolytes after co-sensitization. Therefore, their photovoltaic performance are determined by the energy level position and the charge recombination process. Finally, two extraordinary power conversion efficiencies of 10.21% and 10.42% were achieved for DSSCs utilizing porphyrin dye **FW-1** co-sensitized with **WS-5** based on cobalt and iodine electrolytes.

Conclusions

In summary, two prominent power conversion efficiencies of 10.21% and 10.42% were achieved for DSSCs utilizing porphyrin dye **FW-1** co-sensitized with **WS-5** based on iodine and cobalt electrolytes, respectively, in contrast with most sensitizers that are only effective with a single electrolyte system. The PCE was significantly enhanced with the help of **WS-5** which is able to fill up the absorption valleys of **FW-1** in the ranges of 350–410 nm and 500–600 nm, indicating that **FW-1** & **WS-5** is a new high performance co-sensitization system. Being easy-to-construct, with high performance, this novel kind of porphyrin-based co-sensitized solar cell provides a unique insight in the development of DSSCs.

Experimental Section

Fabrication of dye-sensitized solar cells

All working electrodes used in this work were prepared and modified following the reported procedure.[9] For cobalt redox electrolyte devices, the working electrode was composed of a 7 µm thick TiO_2 film (active area 0.12 cm^2), including a 3 µm transparent layer with 18 NRT and 4 µm scattering layer with 18 NR-AO and the films were then immersed into a 0.2 mM solution of **FW-1** in a mixture of toluene and ethanol (volume ratio of 1: 4) at 25°C for 12 h at room temperature. For iodide redox electrolyte devices, the working electrodes were prepared with a 14 µm thick TiO_2 film (active area 0.12 cm^2), including a 6 µm transparent layer with 18 NRT and 8 µm scattering layer with 18 NR-AO, and then the films were sensitized with **FW-1** similarly to cobalt electrolyte for 2 h at room temperature. For co-sensitization, **FW-1**-sensitized films were washed with ethanol and dried, and then immersed in a solution containing **WS-5** (0.3 mM) in a mixture of chloroform and ethanol (volume ratio of 1: 1) and kept at 25 °C for different time. The Pt counter electrode was prepared by spin-coating with three drops of H_2PtCl_6 solution (0.02 M in 2-propanol solution) on FTO glass and heating at 400°C for 15 min. Before fabrication, a hole (diameter of 0.8 mm) was drilled on it. The perforated sheet was cleaned by ultrasound in an ethanol bath for 10 min. For the assembly of DSSCs, a thermally platinized FTO glass counter electrode and the working electrode were then sealed with a 25 µm thick hot-melt film (Surlyn 1702, DuPont) at 129°C. A drop of electrolyte solution was injected into the cell

through the hole predrilled in counter electrode and then the hole was sealed with aluminum tape. The electrolytes used in this work include cobalt and iodine electrolyte. The former is composed of 0.25 M tris(2,2-bipyridine) cobalt(II) di[bis-(trifluoromethanesulfonyl)imide], 0.05 M tris(2,2′-bipyridine)-cobalt(III) tris[bis(trifluoromethanesulfonyl)imide], 0.5 M 4-tert-butylpyridine (TBP), and 0.1 M lithium bis-(trifluoromethanesulfonyl)imide (LiTFSI) in acetonitrile. The latter (coded as L130) employed was a solution of 0.1 M LiI, 0.05 M I_2, 0.6 M 1-methyl-3-propyl-imidazolium iodide (PMII), and 0.5 M 4-tert-butylpyridine (TBP) in a mixture of acetonitrile and valeronitrile (volume ratio of 85: 15). In this work, all test data shown were the average values of five parallel tests.

Instrumentation

The UV-Vis absorption spectra of sensitizer dyes in solution and adsorbed on titania films were measured on a Varian Cary 100 spectrophotometer. ^{1}H NMR (500 MHz) and ^{13}C NMR (125 MHz) spectra were recorded in deuterated solvents on a Bruker ADVANCE 500 NMR Spectrometer. J values are expressed in Hz and quoted chemical shifts are in ppm downfield from tetramethylsilane (TMS) reference using the residual protonated solvent as an internal standard. The signals have been designated as follows: s (singlet), d (doublet), t (triplet), and m (multiplets). High resolution mass spectra (HRMS) were determined on IonSpec 4.7 Tesla Fourier Transform Mass Spectrometer. The cyclic voltammograms (CV) experiments were recorded with a Versastat II electrochemical workstation (Princeton Applied Research). Photovoltaic measurements were performed by employing an AM 1.5 solar simulator equipped with a 300 W xenon lamp (model no. 91160, Newport). The voltage step and delay time of the photocurrent were 10 mV and 40 ms, respectively. The incident photon-to-charge carrier efficiencies (IPCEs) of all DSSCs were measured on a Newport-74125 system (Newport instruments). The intensity of monochromatic light was detected using a Si detector (Newport-71640). The electrochemical impedance spectroscopy (EIS) measurements of all DSSCs were performed using a Zahner IM6e Impedance Analyzer (ZAHNER-Elektrik GmbH & CoKG, Kronach, Germany), with a frequency range of 0.1 Hz–100 kHz and an alternative signal of 5 mV at a constant temperature of 25°C in the dark conditions. The spectra were characterized using ZView software (Scribner Associates). The OCVD (open circuit voltage decay) curves were also recorded using the same Zahner workstation. In measurements, the voltage of cells reached steady state under illumination by a blue LED with intensity of 80 mW cm^{-2} and then was recorded after switching off the light.

Synthesis

The starting material 1 was purchased from commercial suppliers and used without further purification unless otherwise specified. Compounds 2 [19] and 8 [20] were synthesized according to literature procedures.

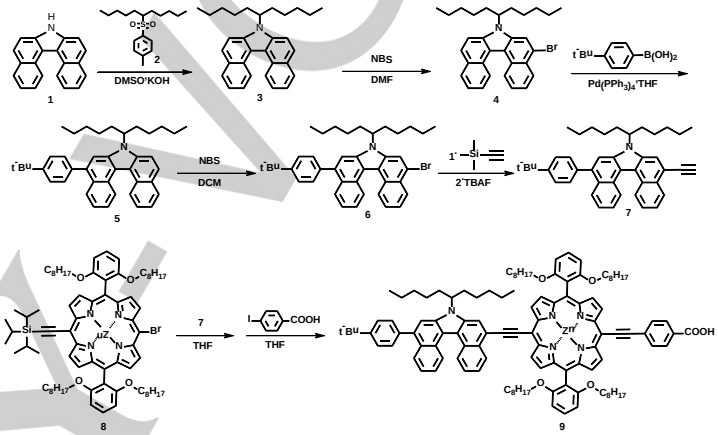

Figure.4 Synthetic route of target dye **FW-1**

Synthesis of compound 3.

A mixture of 1 (410 mg, 1.54 mmol), 2 (1 g, 3.07 mmol) and KOH (774 mg, 13.82 mmol) in 20 mL DMSO was stirred at room temperature for 3 h. The reaction mixture was poured in water and the product was extracted with CH_2Cl_2. The combined organic layers were washed with water and dried over $MgSO_4$. After removal of solvent under vacuum, the residue was purified by silica gel chromatography (dichloromethane: petroether =1:8) to afford compound 3 (510 mg, 79%) as a colourless liquid. ^{1}H NMR (500 MHz, 373 K, $(CD_3)_2SO$, ppm) δ=9.08-9.07 (d, J=8.5 Hz, 2H), 8.09-8.07 (d, J=8.1 Hz 2H), 8.03-8.0 (d, J=8.9 Hz, 2H), 7.94-7.92 (m, J=8.5 Hz, 2H), 7.68-7.65 (t, J=7.0 Hz, 2H), 7.52-7.50 (t, J=7.9 Hz, 2H), 5.06-5.00 (m, 1H), 2.39-2.32 (m, 2H), 2.13-2.06 (m, 2H), 1.21-0.96 (m, 12H), 0.70-0.67 (t, 7.3 Hz, 6H). ^{13}C NMR (125 MHz, $(CD_3)_2SO$, ppm) δ=129.9, 129.5, 129.2, 126.6, 125.7, 124.9, 123.7, 56.9, 41.17, 41.0, 40.8, 40.7, 40.5, 40.3, 40.2, 34.5, 31.4, 26.3, 22.2, 14.0. HRMS (MALDI, 100%) m/z calcd (%) for $C_{31}H_{35}N$: 421.2764, found 421.2763.

Synthesis of compound 4.

Compound 3 (510 mg, 1.21 mmol) was dissolved in DMF (300 ml),

then the NBS (193.76 mg, 1.09 mmol) was slowly added into the solution and stirred at room temperature for 1 h. The reaction mixture was poured in water and the product was extracted with CH_2Cl_2. The combined organic layers were washed with water and dried over $MgSO_4$. After removal of solvent under vacuum, the residue was purified by silica gel chromatography (petroether) to afford compound 4 (545 mg, 90%) as a white solid. ^{1}H NMR (500 MHz, 373 K, $(CD_3)_2SO$, ppm) δ=9.12-9.10 (d, J=8.4 Hz, 1H), 9.01-8.99 (d, J=8.4 Hz 1H), 8..42 (s, 1H), 8.40-8.38 (d, J=6.5 Hz, 1H), 8.11-8.09 (d, J=8.0 Hz, 1H), 8.05-8.04 (d, J=9.0 Hz, 1H), 7.99-7.97 (d, J=9.0 Hz, 1H), 7.78-7.75 (t, J=7.2 Hz, 1H), 7.70-7.65 (m, J=9 Hz, 2H), 7.76-7.52 (t, J=7.3 Hz, 1H), 5.06-5.00 (m, 1H), 2.36-2.29 (m, 2H), 2.14-2.07 (m, 2H), 1.23-0.96 (m, 12H), 0.71-0.68 (t, 7.3 Hz, 6H). ^{13}C NMR (125 MHz, (CD3)2SO, ppm) δ=129.6, 128.2, 127.4, 126.7, 126.1, 125.4, 125.2, 124.8, 124.4, 57.2, 41.2, 41.0, 40.8, 40.7, 40.5, 40.3, 40.2, 34.4, 31.4, 26.3, 22.2, 14.0. HRMS (MALDI, 100%) m/z calcd (%) for $C_{31}H_{34}BrN$: 499.1869, found 499.1866.

Synthesis of compound 5.

To a solution compound 4 (480 mg, 0.96 mmol) and 4-tert-Butylbenzeneboronic acid (256 mg, 1.44 mmol) in THF (20 mL) was added $Pd(PPh_3)_4$ (110 mg, 0.096 mmol), the solution was ventilated with nitrogen for a few minutes. Then sodium carbonate (553 mg, 0.5M) was added, the solution was ventilated with nitrogen for a few minutes. The mixture was stirred at 80°C for 5 h. The reaction mixture was poured in water and the product was extracted with CH_2Cl_2. The combined organic layers were washed with water and dried over MgSO4. After removal of solvent under vacuum, the residue was purified by silica gel chromatography (dichloromethane: petroether =1:4) to afford compound 5 (550 mg, 94%) as a white solid. ^{1}H NMR (500 MHz, 373 K, $(CD_3)_2SO$, ppm) δ=9.14-9.12 (d, J=8.4 Hz, 1H), 9.09-9.07 (d, J=8.5 Hz 1H), 8.10-8.08 (d, J=7.9 Hz, 1H), 8.04-8.03 (d, J=9.0 Hz, 1H), 7.98-7.94 (m, 2H), 7.90 (s, 1H), 7.70-7.69 (m, 2H), 7.63-7.61 (d, J=8.3 Hz, 2H), 7.56-7.51 (m, 3H), 7.47-7.44 (m, 1H), 5.08-5.04 (m, 1H), 2.38-2.31 (m, 2H), 2.12-2.05 (m, 2H), 1.44 (s, 9H), 1.25-0.97 (m, 12H), 0.70-0.67 (t, J=7.3 Hz, 6H). ^{13}C NMR (125 MHz, (CD3)2SO, ppm) δ=130.3, 129.9, 129.6, 129.2, 128.3, 127.4, 126.7, 125.8, 125.6, 125.3, 124.9, 123.9, 123.8, 56.9, 41.2, 41.0, 40.9, 40.7, 40.5, 40.4, 40.2, 34.5, 34.5, 31.9, 31.4, 26.3, 22.2, 14.0. HRMS (MALDI, 100%) m/z calcd (%) for $C_{41}H_{47}N$: 553.3703, found 553.3700.

Synthesis of compound 6.

The solution of compound 5 (550 mg, 0.97 mmol) and NBS (180 mg, 1.01 mmol) in CH_2Cl_2 (30 mL) was stirred at room temperature for 0.5 h. The reaction mixture was poured in water and the product was extracted with CH_2Cl_2. The combined organic layers were washed with water and dried over $MgSO_4$. After removal of solvent under vacuum, the residue was purified by silica gel chromatography (dichloromethane: petroether =1:4) to afford compound 6 (530 mg, 84%) as a yellow solid. ^{1}H NMR (500 MHz, 373 K, $(CD_3)_2SO$, ppm) δ=9.05-9.00 (m, 2H), 8.44 (s, 1H), 8.42-8.40 (d, J=8.4 Hz, 1H), 8.07-8.06 (d, J=2.1 Hz, 1H), 7.97 (s, 1H), 7.82-7.70 (m, 2H), 7.70-7.64 (m, 4H), 7.54-7.53 (d, J=8.2 Hz, 2H), 5.10-5.07 (m, 1H), 2.34-2.26 (m, 2H), 2.12-2.05 (m, 2H), 1.44 (s, 9H), 1.22-0.98 (m, 12H), 0.70-0.68 (t, J=7.3 Hz, 6H). ^{13}C NMR (125 MHz, $(CD_3)_2SO$, ppm) δ=130.2, 129.6, 129.2, 128.7, 128.3, 127.3, 126.0, 125.5, 125.3, 57.2, 41.2, 41.0, 40.8, 40.7, 40.5, 40.3, 40.2, 34.4, 31.9, 31.4, 26.2, 22.2, 14.0. HRMS (MALDI, 100%) m/z calcd (%) for $C_{41}H_{46}BrN$: 631.2808, found 631.2806.

Synthesis of compound 7.

Compound 6 (530 mg, 0.82 mmol), trimethylsilyacetylene (210 mg, 2.05 mmol), $Pd(PPh_3)_2Cl_2$ (110 mg, 0.16 mmol), Et_3N (1 ml) and CuI (47 mg, 0.25 mmol) were added into a glass pressure vessel in dry THF (3 ml) under nitrogen atmosphere. The mixture reaction was stirred at 80°C for 5 h. After removal of solvent under vacuum, the residue was purified by silica gel chromatography (dichloromethane: petroether =1:10) to afford intermediate as an orange solid. The intermediate was dissolved in THF, TBAF was added. The mixture solution was stirred under nitrogen atmosphere for 0.5 h. The reaction mixture was poured in water and the product was extracted with CH_2Cl_2. The combined organic layers were washed with water and dried over $MgSO_4$. After removal of solvent under vacuum to afford compound 7 (360 mg, 76%) as a yellow solid. ^{1}H NMR (500 MHz, 373 K, $(CD_3)_2SO$, ppm) δ=9.12-9.08 (m, 2H), 8.53-8.51 (d, J=8.1 Hz 1H), 8.28 (s, 1H), 8.00-7.96 (d, J=8.4 Hz, 1H), 7.91 (s, 1H), 7.77-7.74 (t, J=8.0 Hz, 1H), 7.71-7.62 (m, 4H), 7.54-7.53 (d, J=7.8 Hz, 2H), 7.50-7.47 (t, J=8.1 Hz, 1H), 5.11-5.50 (m, 1H), 4.46 (s, 9H), 2.36-2.28 (m, 2H), 2.13-2.01 (m, 2H), 1.44 (s, 1H), 1.25-1.01 (m, 12H), 0.70-0.68 (t, J=7.3Hz, 6H). ^{13}C NMR (125 MHz, $(CD_3)_2SO$, ppm) δ=130.3, 127.6, 127.2, 126.4, 126.0, 125.8, 125.4, 125.2, 124.9, 124.3, 57.0, 41.2, 41.0, 40.8, 40.7, 40.5, 40.3, 40.2, 34.5, 31.8, 31.4, 26.3, 22.2, 14.0. HRMS (MALDI, 100%) m/z calcd (%) for $C_{41}H_{47}N$: 577.3703, found 577.3703.

Synthesis of compound **FW-1**.

Compound 7 (118 mg, 0.2 mmol), compound 8 (180 mg, 0.14mmol), $Pd(PPh_3)_2Cl_2$ (20 mg, 0.03 mmol), Et_3N (3 ml) and CuI (8 mg, 0.04 mmol) were added into a glass pressure vessel in dry

THF under nitrogen atmosphere. The mixture reaction was stirred at 80°C overnight. The mixture reaction was concentrated, the residue was purified by silica gel chromatography (dichloromethane: petroether =1:4) to afford intermediate. The intermediate was dissolved in THF, and TBAF was added. The mixture solution was stirred under nitrogen atmosphere for 0.5 h. The reaction mixture was poured in water and the product was extracted with CH_2Cl_2. The combined organic layers were washed with water and dried over $MgSO_4$. After removal of solvent under vacuum to afford the residue (150 mg) without further purification. The residue and 4-iodobenzoic acid (104 mg, 0.42 mmol) solution was degassed with dinitrogen for 10 min; $Pd_2(dba)_3$ (21 mg, 0.023 mmol) and $AsPh_3$ (46 mg, 0.15 mmol) were added to the mixture. The solution was refluxed for 4 h under dinitrogen. The solvent was removed under reduced pressure. The residue was purified by silica gel chromatography (dichloromethane: methanol=20:1) to afford compound **FW-1** (120 mg, 49%) as a green solid. ^{1}H NMR (500 MHz, 373 K, $(CD_3)_2SO$, ppm) δ=9.76-9.75 (d, J=4.4 Hz, 2H), 9.58-9.57 (d, J=4.5 Hz, 2H) 9.27-9.21 (m, 2H), 8.77-8.73 (m, J=8.1 Hz, 4H), 8.19-8.17 (d, J=8.3 Hz, 2H), 8.13-8.12 (d, J=8.4 Hz, 2H), 8.04-8.02 (d, J=8.2 Hz, 1H), 8.00 (s, 1H), 7.90-7.84 (m, 3H), 7.78-7.74 (m, 4H), 7.67-7.66 (d, J=8.3 Hz, 2H), 7.60-7.59 (d, J=8.3 Hz , 2H), 7.55-7.52 (t, J=7.1 Hz , 1H), 7.15-7.14 (d, J=8.6 Hz , 4H), 5.31-5.23 (m, 1H), 3.89-3.86 (t, J=6.4 Hz , 8H), 2.28-2.18 (m, 4H), 1.46(s, 9H), 1.33-1.18 (m, 12H), 1.02-0.49 (m, 68H). ^{13}C NMR (100 MHz, $CDCl_3$, ppm) δ = 170.3, 160.0, 151.9, 151.7, 150.8, 150.7, 138.7, 132.3, 132.0, 131.1, 130.9, 130.5, 130.2, 130.1, 130.0, 130.0, 127.9, 125.6, 125.3, 121.0, 115.7, 105.4, 101.6, 99.1, 68.8, 34.9, 34.7, 31.8, 31.7, 31.6, 31.4, 29.7, 28.7, 28.7, 26.7, 25.3, 22.5, 22.5, 22.3, 14.0, 13.8. HRMS (MALDI, 100%) m/z calcd (%) for $C_{116}H_{133}N_5O_6Zn$: 1755.9542, found 1755.9535.

Acknowledgements

This work was supported by NSFC for Creative Research Groups (21421004), the Programme of Introducing Talents of Discipline to Universities(B16017) and Distinguished Young Scholars (21325625), NSFC/China, Oriental Scholarship, Fundamental Research Funds for the Central Universities (WJ1416005 and WJ1315025), and the Scientific Committee of Shanghai (14ZR1409700 and 15XD1501400) for financial support.

Keywords: Duplexing • porphyrin • redox shuttle • co-sensitizer • dye-sensitized solar cells

[1] B. O'Regan and M. Grätzel, *Nature*, **1991**, *353*, 737-740.

[2] a) M. Grätzel, *Nature*, **2001**, *414*, 338–344; b) T. W. Hamann and J. W. Ondersma, *Energy Environ. Sci.*, **2011**, *4*, 370–381; c) K. L. Wu, S. T. Ho, C. C. Chou, Y. C. Chang, H. A. Pan, Y. Chi and P. T. Chou, *Angew. Chem., Int. Ed.*, **2012**, *51*, 5642-5646; d) S. Jiang, X. Lu, G. Zhou and Z. S. Wang, *Chem. Commun.*, **2013**, *49*, 3899–3901; e) Q. Feng, X. Jia, G. Zhou and Z. S. Wang, *Chem. Commun.*, **2013**, *49*, 7445–7447; f) S. F. Zhang, X. D. Yang, Y. Numata and L. Y Han, *Energy Environ. Sci.*, **2013**, *6*, 1443–1464; g) X. Li, S. C. Cui, D. Wang, Y. Zhou, H. Zhou, Y. Hu, J. G. Liu, Y. T. Long, W. J. Wu, J. L. Hua, H. Tian, *Chemsuschem*, **2014**, *7*, 2879–2888; h) M. Kouhnavard, N. A. Ludin, B. V. Ghaffari, K. Sopian, S. Ikeda, *Chemsuschem*, **2015**, *8*, 1510–1533; i) V. S. Manthou, E. K. Pefkianakis, P. Falaras, G. C. Vougioukalakis, *Chemsuschem*, **2015**, *8*, 588–599.

[3] a) M. Grätzel, R. A. J. Janssen, D. B. Mitzi, and E. H. Sargent, *Nature*, **2012**, *488*, 304–312; b) S. W. Wang, K. L. Wu, E. Ghadiri, M. G. Lobello, S. T. Ho, Y. Chi, J. E. Moser, F. D. Angelis, M. Grätzel and M. K. Nazeeruddin, *Chem. Sci.*, **2013**, *4*, 2423–2433; c) Y. S. Xie, W. J. Wu, H. B. Zhu, J. C. Liu, W. W. Zhang, H. Tian, and W. H. Zhu, *Chem. Sci.*, **2016**, *7*, 544–549; d) W. J. Ying, J. B. Yang, M. Wielopolski, T. Moehl, J. E. Moser, P. Comte, J. L. Hua, S. M. Zakeeruddin, H. Tian and M. Grätzel, *Chem. Sci.,* **2014**, *5*, 206–214; e) E. Bi, Y. J. Su, H. Chen, X. D. Yang, M. S. Yin, F. Ye, Z. L. Li and L. Y. Han, *RSC Adv.*, **2015**, *5*, 9075–9078; f) T. Edvinsson, C. Li, N. Pschirer, J. Schöneboom, F. Eickemeyer, R. Sens, G. Boschloo, A. Herrmann, K. Müllen, and A. Hagfeldt, *J. Phys. Chem. C*, **2007**, *111*, 15137-15140; g) M. Zhang, J. Y. Liu, Y. H. Wang, D. F. Zhou and P. Wang, *Chem. Sci.*, **2011**, *2*, 1401–1406; h) C. Li, M. Y. Liu, N. G. Pschirer, M. Baumgarten, and K. Müllen, *Chem. Rev*. **2010**, *110*, 6817–6855.

[4] a) C. Y. Lin, C. F. Lo, L. Luo, H. P. Lu, C. S. Hung and E. W. G. Diau, *J. Phys. Chem. C*, **2009**, *113*, 755-764; b) J. K. Park, J. Chen, H. R. Lee, S. W. Park, H. Shinokubo, A. Osuka and D. Kim, *J. Phys. Chem. C*, **2009**, *113*, 21956-21963; c) M. V. Martínez-Díaz, G. dela Torre and T. Torres, *Chem. Commun.*, **2010**, *46*, 7090-7108; d) L. L. Li and E. W. G. Diau, *Chem. Soc. Rev.*, **2013**, *42*, 291-304; e) H. Imahori, T. Umeyama and S. Ito, *Acc. Chem. Res.*, **2009**, *42*, 1809-1818; f) T. Higashino and H. Imahori, *Dalton Trans.*, **2015**, *44*, 448-463; g) M. Urbani, M. Grätzel, M. K. Nazeeruddin and T. S. Torres, *Chem. Rev.*, **2014**, *114*, 12330-12396; f) R. G. W. Jinadasa, B. Li, B. Schmitz, S. Kumar, Y. Hu, L. Kerr, H. Wang, *Chemsuschem*, **2016**, *9*, 2239–2249

[5] S. Mathew, A. Yella, P. Gao, R. H. Baker, B. F. E. Curchod, T. I. Astani, U. Rothlisberger, M. K. Nazeeruddin and M. Grätzel, *Nat. Chem.*, **2014**, *6*, 242–247.

[6] a) Y. Z. Wu, W. H. Zhu, S. M. Zakeeruddin and M. Grätzel, *ACS Appl. Mater, Interfaces*, **2015**, *7*, 9307-9318; b) W. H. Zhu, Y. Z. Wu, S. T. Wang, W. Q. Li, X. Li, J. Chen, Z. S. Wang and H. Tian, *Adv. Funct. Mater.*, **2011**, *21*, 756-763; c) Y. Cui, Y. Z. Wu, X. F. Lu, X. Zhang, G. Zhou, F. B. Miapeh, W. H. Zhu and Z. S. Wang, *Chem. Mater.*, **2011**, *23*, 4394-4401; d) W. Q. Li, Y. Z. Wu, Q. Zhang, H. Tian and W. H. Zhu, *ACS Appl. Mater. Interfaces*, **2012**, *4*, 1822-1830; e) Y. Z. Wu, M. Marszalek, S. M. Zakeeruddin, Q. Zhang, H. Tian, M. Grätzel and W. H. Zhu, *Energy Environ. Sci.*, **2012**, *5*, 8261-8272; f) Q. P. Chai, W. Q. Li, J. C. Liu, Z. Y. Geng, H. Tian, W. H. Zhu, *Sci. Rep.*, **2015**, *5*, 11330; g) H. B. Zhu, B. Liu, J. C. Liu, W. W. Zhang and W. H. Zhu, *J. Mater. Chem. C*, **2015**, *3*, 6882-6890.

[7] W. Q. Li, Y. Z. Wu, Q. Zhang, H. Tian and W. H. Zhu, *ACS Appl. Mater. Interfaces*, **2012**, *4*, 1822-1830.

[8] a) Y. Y. Tang, Y. Q. Wang, X. Li, H. Ågren, W. H. Zhu and Y. S. Xie, *ACS Appl. Mater. Interfaces*, **2015**, *7*, 27976–27985; b) J. C. Liu, B.

Liu, Y. Y. Tang, W. W. Zhang, W. J. Wu, Y. S. Xie and W. H. Zhu, *J. Mater. Chem. C*, **2015**, *3*, 11144–11150.

[9] Y. S. Xie, Y. Y. Tang, W. J. Wu, Y. Q. Wang, J. C. Liu, X. Li, H. Tian and W. H. Zhu, *J. Am. Chem. Soc.*, **2015**, *137*, 14055–14058.

[10] S. A. Sapp, C. M. Elliott, C. Contado, S. Caramori and A. Bignozzi, *J. Am. Chem. Soc.*, **2002**, *124*, 11215–11222.

[11] a) H. P. Wu, Z. W. Ou, T. Y. Pan, C. M. Lan, W. K. Huang, H. W. Lee, N. M. Reddy, C. T. Chen, W. S. Chao and C. Y. Yeh, *Energy Environ. Sci.*, **2012**, *5*, 9843–9848; b) S. Chang, H. Wang, Y. Hua, Q. Li, X. Xiao, W. K. Wong, W. Y. Wong, X. Zhu and T. Chen, *J. Mater. Chem. A.*, **2013**, *1*, 11553–11558.

[12] A. J. Frank, N. Kopidakis and J. van de Lagemaat, *Chem. Rev.*, **2004**, *248*, 1165–1179.

[13] Y. M. Cao, Y. Bai, Q. J. Yu, Y. M. Cheng, S. Liu, D. Shi, F. F. Gao and P. J. Wang, *J. Phys. Chem. C*, **2009**, *113*, 6290-6297.

[14] A. Hagfeldt, G. Boschloo, L. Sun, L. Kloo and H. Pettersson, *Chem. Rev.*, **2010**, *110*, 6595-6663.

[15] a) H. Nusbaumer, J. E. Mose, S. M. Zakeeruddin, M. K. Nazeeruddin and M. Grätzel, *J. Phys. Chem. B*, **2001**, *105*, 10461-10464; b) K. B. Aribia, T. Moehl, S. M. Zakeeruddin and M. Grätzel , *Chem. Sci.*, **2013**, *4*, 454-459.

[16] H. X. Wang, P. G. Nicholson, L. Peter, S. M. Zakeeruddin and M. Grätzel, *J. Phys. Chem. C*, **2010**, *114*, 14300-14306.

[17] J. B. Yang, P. Ganesan, J. Teuscher, T. Moehl, Y. J. Kim, C. Y. Yi, P. Comte, K. Pei, T. W. Holcombe and M. K. Nazeeruddin, *J. Am. Chem. Soc.*, **2014**, *136*, 5722–5730.

[18] C. Y. Yi, F. Giordano, N. L. Cevey-Ha, H. N. Tsao, S. M. Zakeeruddin, and M. Grätzel, *Chemsuschem*, **2014**, *7*, 1107–1113.

[19] [18]T. Taguri, R. Yamakawa, T. Fujii, Y. Muraki and T. Ando, *Tetrahedron: Asymmetry,* **2012**, *23*, 852–858.

[20] [19]A. Yella, H. W. Lee, H. N. Tsao, C. Y. Yi, A. K. Chandiran, M. K. Nazeeruddin, E. W. G. Diau, C. Y. Yeh, S. M. Zakeeruddin, M. Grätzel, *Science*, **2011**, *334,* 629-634.

Entry for the Table of Contents (Please choose one layout)

FULL PAPER

The improvement of flexibility about choice of electrolyte with co-sensitizer, is also a significant issue for the development of DSSCs. By means of co-sensitization in this work, significantly compensating the UV-vis adsorption spectra and change the charge recombination inhibition, we got high efficiency of 10.21% and 10.42%, respectively, for electrolyte based on iodine or cobalt redox.

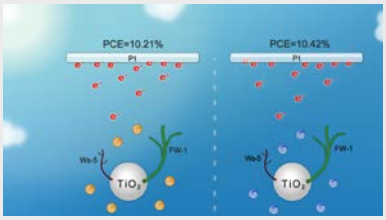

Huaide Xiang, Wei Fan, Jia Hui Li, Tianyue Li, Neil Robertson, Xiongrong Song, Wenjun Wu, Zhaohui Wang, Weihong Zhu, and He Tian**

Page No. – Page No.

High performance porphyrin-based dye-sensitized solar cells with both iodine and cobalt redox shuttles